# Radiation characteristics of rectangular patch antennas with a laminated ground plane

J.-F. Kiang

*Indexing terms: Patch radiator, Microstrip antenna, Laminated ground plane, Input impedance, Radiation pattern*

**Abstract:** In modern aeronautical and automobile industries, composite materials are becoming increasingly popular for building the vehicular surface. The antenna engineer may face the situation of needing to design patch radiators above the composite material instead of a conductor ground plane. The input impedance and radiation patterns of a rectangular patch antenna attached to a laminated ground plane by using an integral equation approach is studied herein. The effects of composite lamina, substrate thickness and current probe location on the input impedance and radiation patterns are analysed. It is observed that the bandwidth of the patch antenna can be increased significantly when the substrate thickness is reduced. This observation is contrary to the conventional microstrip antenna concept and can be used to design a wideband microstrip radiator.

## 1 Introduction

Conventionally, microstrip patch radiators are built as low-profile radiating elements where a metal patch is attached to a substrate with a perfectly conducting ground plane [1–4]. A surface impedance approach has been used to model the imperfect conductor in a layered medium [5]. In [6], the current distribution inside imperfect conductors of finite thickness is considered when analysing the attenuation properties of microstrip lines.

In modern aircraft and vehicle designs, composite materials have been widely used in the vehicle surface to reduce the weight or the radar cross-section. G/E composite is one example which is made of several laminae of epoxy resin with conductive graphite fibres embedded in specific orientations [7]. If a patch resonator is built on a composite surface, details of the ground plane will affect its radiation properties.

Scattering from a sandwiched layer of conducting fibres has been analysed [8]. If the fibre spacing is comparable to the wavelength, Floquet modes should be incorporated in the analysis. In [7], an anisotropic conductivity tensor is used to study the shielding effectiveness of a G/E composite. The fibre separation in each G/E lamina is a tiny fraction of a wavelength, hence using an equivalent conductivity tensor is appropriate to analyse its propagation properties.

The characteristics of a patch resonator on an anisotropic substrate have been analysed by several authors [9–12]. In [10], a differential matrix operator is derived from the Maxwell equations to calculate the tangential field components. This method was also used in optics [13, 14] and scattering [15]. General derivations can also be found in [16–18].

In this paper we will study the effects of a laminated ground plane on the input impedance and radiation pattern of a rectangular patch radiator. First, a transition matrix will be formulated to model the laminated ground plane. Assume that the wire/fibre spacing in each lamina of the ground plane is much smaller than a wavelength, hence each lamina can be modelled as an anisotropic layer with a conductivity tensor. An integral equation is then derived based on the electric surface current on the rectangular patch. Galerkin's method is applied to solve for the current distribution. The input impedance is then obtained by a variational approach, and the stationary phase approximation is applied to calculate the far field pattern.

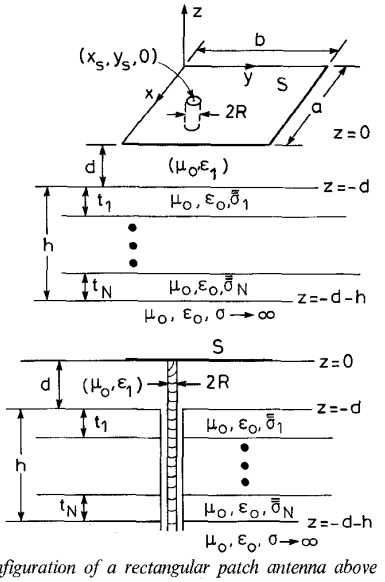


**Fig. 1** *Configuration of a rectangular patch antenna above a laminated ground plane*

## 2 Transition matrix

Fig. 1, shows a rectangular patch radiator above a laminated ground. A substrate is sandwiched between



*IEE Proceedings* online no. 19960232

Paper first received 23rd May 1995 and in revised form 6th November 1995

The author is with the Department of Electrical Engineering, National Chung-Hsing University, Taichung, Taiwan, Republic of China

the patch and the ground. The coaxial cable feeding the patch runs through the laminated ground. The outer conductor is flush with the bottom of the substrate, and the inner conductor of radius $R$ is connected to the rectangular patch. The ground plane is modelled as $N$ laminae of homogeneous anisotropic media stacked along the $z$-direction. The principal axes of each lamina lie in the $xy$ plane, and an effective conductivity tensor, $\bar{\bar{\sigma}}$, is used to describe the electrical properties of each lamina.

We first derive the transition matrix in the spectral domain for a single lamina. If the principal axis of $\bar{\bar{\sigma}}$ skews from the $x$-axis by an angle $\alpha$ (fibres are laid from the $x$-axis by an angle $a$), $\bar{\bar{\sigma}}$ can then be expressed as [7]

$$\bar{\bar{\sigma}} = \begin{bmatrix} \bar{\bar{\sigma}}_s & 0 \\ 0 & \sigma_{zz} \end{bmatrix} = \begin{bmatrix} \sigma_{xx} & \sigma_{xy} & 0 \\ \sigma_{yx} & \sigma_{yy} & 0 \\ 0 & 0 & \sigma_{zz} \end{bmatrix} \quad (1)$$

where $\bar{\bar{\sigma}}_s$ is a $2 \times 2$ tensor. $\sigma_{xx} = \sigma'_{xx} \cos^2 \alpha + \sigma'_{yy} \sin^2 \alpha$, $\sigma_{xy} = \sigma_{yx} = (\sigma'_{yy} - \sigma'_{xx}) \sin \alpha \cos \alpha$, $\sigma_{yy} = \sigma'_{xx} \sin^2 \alpha + \sigma'_{yy} \cos^2 \alpha$, and $\sigma_{zz} = \sigma'_{zz}$. Here, $\sigma'_{xx}$, $\sigma'_{yy}$ and $\sigma'_{zz}$ are conductivities measured along the principal axes of the medium. An isotropic permittivity of $\varepsilon_o$ and an isotropic permeability of $\mu_o$ are assumed in the whole medium.

The $\bar{E}$-field, $\bar{H}$-field, and the curl operator can be decomposed into the $z$ component and $s$ ($x$ and $y$) components. Eliminating $\bar{E}_z$ and $\bar{H}_z$ from Maxwell's equations, and assuming asolution with the $xy$ dependence of exp ($i\bar{k}_s \cdot \bar{r}_s$) ($\bar{k}_s = \hat{x}k_x + \hat{y}k_y$, $\bar{r}_s = \hat{x}x + \hat{y}y$), the following state-variable equations are obtained:

$$\frac{\mathrm{d}}{\mathrm{d}z} \bar{V}(\bar{k}_s, z) = \bar{\bar{H}}(\omega, \bar{k}_s, \bar{\bar{\sigma}}) \cdot \bar{V}(\bar{k}_s, z) \quad (2)$$

where

$$\bar{V}(\bar{k}_s, z) = [E_x(\bar{k}_s, z), E_y(\bar{k}_s, z), H_x(\bar{k}_s, z), H_y(\bar{k}_s, z)]^t$$

To solve eqn. 2, first segment the thickness ($z$) coordinate into small divisions of size $\Delta z$, then approximate the derivative with respect to $z$ by a finite difference form [15]. Thus the tangential fields at $z$ and $z + \Delta z$ can be related by a matrix. By multiplying all these matrices from $z = z_0$ to $z = z_N$, we obtain a transition matrix $\bar{\bar{P}}(\bar{k}_s; z_N, z_0)$ to relate the tangential field components at $z = z_N$ and $z = z_0$ as

$$\bar{V}(\bar{k}_s, z_N) = \bar{\bar{P}}(\bar{k}_s; z_N, z_0) \cdot \bar{V}(\bar{k}_s, z_0) \quad (3)$$

## 3 Rectangular patch radiator

The $z$-component of the fields in region (0) ($z \geq 0$) can be expressed as

$$\begin{aligned} E_{0z}(\bar{r}) &= \int\int_{-\infty}^{\infty} d\bar{k}_s e^{i\bar{k}_s \cdot \bar{r}_s} e_0(\bar{k}_s) e^{ik_{0z} z_0} \\ H_{0z}(\bar{r}) &= \int\int_{-\infty}^{\infty} d\bar{k}_s e^{i\bar{k}_s \cdot \bar{r}_s} h_0(\bar{k}_s) e^{ik_{0z} z_0} \end{aligned} \quad (4)$$

where $z_0 = z$, $z_1 = z + d$. Here $E_{0z}(\bar{r})$ ($H_{0z}(\bar{r})$) is represented as a superposition of upward-propagating waves with wavevector $\bar{k}_s + \hat{z}k_{0z}$ and amplitude $e_0(\bar{k}_s)$ ($h_0(\bar{k}_s)$). The field components $E_{1z}(\bar{r})$ and $H_{1z}(\bar{r})$ in region (1) ($-d \leq z \leq 0$) can be similarly represented. The tangential (to $z$) field components can be derived from $E_{0z}(\bar{r})$, $H_{0z}(\bar{r})$, $E_{1z}(\bar{r})$ and $H_{1z}(\bar{r})$ [19].

The tangential field components at $z = z_N = -d$ and $z = z_0 = -\mathrm{d} - h$ are related by the transition matrix as

$$\begin{bmatrix} \bar{E}_{1s}(\bar{r}_s, z_N) \\ \bar{H}_{1s}(\bar{r}_s, z_N) \end{bmatrix} = \int\int_{-\infty}^{\infty} d\bar{k}_s e^{i\bar{k}_s \cdot \bar{r}_s} \bar{\bar{P}}(\bar{k}_s; z_N, z_0) \cdot \begin{bmatrix} \bar{E}_s(\bar{k}_s, z_0) \\ \bar{H}_s(\bar{k}_s, z_0) \end{bmatrix} \quad (5)$$

where the subscript $s$ means the tangential (to $z$) components.

Next, we impose the boundary conditions that: (1) the tangential electric field at $z = -d - h$ vanishes; (2) the tangential electric fields are continuous across the boundary at $z = 0$; (3) the tangential electric fields and magnetic fields are continuous across the boundary at $z = -d$; and (4) the discontinuity of tangential magnetic fields at $z = 0$ accounts for the surface current. Thus, the tangential electric field at $z = 0$ can be expressed in terms of the spectral representation of patch surface current, $\bar{J}_s(\bar{k}_s)$, as

$$\bar{E}_s(\bar{r}_s) = \int\int_{-\infty}^{\infty} d\bar{k}_s e^{i\bar{k}_s \cdot \bar{r}_s} \bar{\bar{G}}(\bar{k}_s) \cdot \bar{J}_s(\bar{k}_s) \quad \bar{r}_s \text{ on } S \quad (6)$$

where $\bar{\bar{G}}$ is the dyadic which expresses the tangential electric field on the patch in terms of the surface current on the same patch.

## 4 Integral equation

To calculate the input impedance of the patch radiator, we first assume that the current distribution along the probe is uniform in the $z$ direction as

$$\bar{J}(\bar{r}) = \hat{z} I_0 \delta(x - x_s)\delta(y - y_s) \qquad -d \leq z \leq 0 \quad (7)$$

The tangential electric field at $z = 0$ generated by this current distribution can be expressed as

$$\bar{E}_{1s}^{(p)}(\bar{r}_s, z = 0) = \int\int_{-\infty}^{\infty} d\bar{k}_s e^{i\bar{k}_s \cdot (\bar{r}_s - \bar{r}'_s)} \bar{e}_1^{(p)}(\bar{k}_s) \quad (8)$$

where $\bar{r}'_s = \hat{x}x_s + \hat{y}y_s$, $\bar{e}_1^{(p)}(\bar{k}_s)$ is the tangential field spectral vector contributed by the current distribution in eqn. 7.

Next, imposing the boundary condition that the total tangential electric field on the rectangular patch vanishes to obtain the following integral equation

$$\int\int_{-\infty}^{\infty} d\bar{k}_s e^{i\bar{k}_s \cdot \bar{r}_s} \bar{\bar{G}}(\bar{k}_s) \cdot \bar{J}_s(\bar{k}_s) = -\int\int_{-\infty}^{\infty} d\bar{k}_s e^{i\bar{k}_s \cdot (\bar{r}_s - \bar{r}'_s)} \bar{e}_1^{(p)}(\bar{k}_s) \quad \bar{r} \text{ on } S \quad (9)$$

## 5 Numerical scheme

To apply Galerkin's method to solve eqn. 9 for the current distribution, we first choose a set of basis functions to represent the surface current as

$$\bar{J}_s(\bar{r}_s) = \hat{x} \sum_{n=1}^{N_{x1}} \sum_{m=0}^{M_{x1}} a_{nm}^x f_{nm}^x(\bar{r}_s) + \hat{y} \sum_{n=0}^{N_{y1}} \sum_{m=1}^{M_{y1}} a_{nm}^y f_{nm}^y(\bar{r}_s) \quad (10)$$

where

$$f_{nm}^x(\bar{r}_s) = \begin{cases} \sin(\alpha_n x)\cos(\beta_m y) & 0 \leq x \leq a,\ 0 \leq y \leq b \\ 0 & \text{elsewhere} \end{cases}$$

$$f_{nm}^y(\bar{r}_s) = \begin{cases} \cos(\alpha_n x)\sin(\beta_m y) & 0 \leq x \leq a,\ 0 \leq y \leq b \\ 0 & \text{elsewhere} \end{cases} \quad (11)$$

with $\alpha_n = n\pi/a$ and $\beta_m = m\pi/b$. Take the Fourier transform of eqn. 10 and substitute it into eqn. 9. Next, choose the same set of basis functions as weighting functions, and take the inner product of each weighting function with the integral eqn. 9 to obtain

$$\sum_{\beta=x,y}\sum_{n=N_\beta}^{N_{\beta 1}}\sum_{m=M_\beta}^{M_{\beta 1}} a_{nm}^{\beta} \times \int\int_{-\infty}^{\infty} d\bar{k}_s \tilde{f}_{kl}^{\alpha}(-\bar{k}_s)\hat{\alpha}\cdot\bar{\bar{G}}(\bar{k}_s)\cdot\hat{\beta}\tilde{f}_{nm}^{\beta}(\bar{k}_s) = -\int\int_{-\infty}^{\infty} d\bar{k}_s e^{-i\bar{k}_s\cdot\bar{r}_s'}\tilde{f}_{kl}^{\alpha}(-\bar{k}_s)\hat{\alpha}\cdot\bar{e}_1^{(p)}(\bar{k}_s) \quad (12)$$

$$\alpha = x, y;\ N_\alpha \le k \le N_{\alpha_1};\ M_\alpha \le l \le M_{\alpha_1}$$

where

$$N_\beta = \begin{cases} 1 & \beta = x \\ 0 & \beta = y \end{cases} \qquad M_\beta = \begin{cases} 0 & \beta = x \\ 1 & \beta = y \end{cases} \quad (13)$$

Eqn. 12 constitutes a matrix equation to be solved for the unknown coefficients.

## 6 Input impedance and radiation pattern

The input impedance can be decomposed into two parts

$$Z_{in} = Z_p + Z_D \quad (14)$$

where $Z_p$ is contributed by the current probe itself, and $Z_D$ is contributed by the surface currents on patch $S$. Using the line current source will give divergent $Z_p$, hence we need to consider the current probe radius $R$ when calculating the self-impedance $Z_p$. Assume that the current density is constant on the probe cylinder surface

$$\bar{J}(\bar{r}) = \hat{z}\frac{I_0}{2\pi R}\delta(|\bar{r}_s - \bar{r}_s'| - R) \qquad -d \le z \le 0 \quad (15)$$

The $z$-component of the electric field on the probe surface generated by this current distribution, $E_z^{(p)}$, is derived first, and is substituted into a stationary formula for the input impedance [20] to obtain the self-impedance

$$Z_p = -\frac{1}{I_0^2}\int_0^{2\pi} R\,d\phi\int_{-d}^{0} dz\frac{I_0}{2\pi R}E_z^{(p)}(\bar{r}_s, z) \quad (16)$$

$$= \frac{\omega\mu_o}{8\pi^2}\int\int_{-\infty}^{\infty} d\bar{k}_s J_0^2(k_s R)\frac{k_s^2}{k_1^2}\frac{1}{k_{1z}} \times\left\{\left[\frac{2idk_1^2}{k_{1z}k_s^2} + \frac{2}{k_{1z}^2}(1 - e^{ik_{1z}d})\right] + \frac{\sin k_{1z}d}{k_{1z}}\int_{-d}^{0} dz'(\tilde{e}_1^U + \tilde{e}_1^D) + \frac{i(1-\cos k_{1z}d)}{k_{1z}}\int_{-d}^{0} dz'(\tilde{e}_1^U - \tilde{e}_1^D)\right\}$$

where $\tilde{e}_1^U$ and $\tilde{e}_1^D$ are the spectral components of electric field in region (1) generated by the probe current. The impedance contributed by the current on $S$ can also be derived using the stationary fomula in [20] to be

$$Z_D = -\frac{[1,0]}{I_0}\cdot\int\int_{-\infty}^{\infty} d\bar{k}_s e^{i\bar{k}_s\cdot\bar{r}_s'} \times\left\{\left(\frac{\sin k_{1z}d}{k_{1z}}\bar{\bar{Y}}_1 + \frac{i(1-\cos k_{1z}d)}{k_{1z}}\bar{\bar{Y}}_2\right)\cdot\left[\begin{matrix}\sum_{n=1}^{N_{x1}}\sum_{m=0}^{M_{x1}} a_{nm}^x\tilde{f}_{nm}^x(\bar{k}_s) \\ \sum_{n=0}^{N_{y1}}\sum_{m=1}^{M_{y1}} a_{nm}^y\tilde{f}_{nm}^y(\bar{k}_s)\end{matrix}\right]\right\} \quad (17)$$

where $\bar{\bar{Y}}_1$ and $\bar{\bar{Y}}_2$ are dyadics related to $\bar{\bar{G}}(\bar{k}_s)$.

Finally, apply stationary phase approximation to calculate the far field pattern. Define

$$\bar{U}_z^{(D)}(\bar{r}) = \begin{bmatrix} E_z^{(D)}(\bar{r}) \\ H_z^{(D)}(\bar{r}) \end{bmatrix} = \int\int_{-\infty}^{\infty} d\bar{k}_s e^{i\bar{k}_s\cdot\bar{r}_s}\begin{bmatrix} e_0(\bar{k}_s) \\ h_0(\bar{k}_s)\end{bmatrix} e^{ik_{0z}z_0} \approx -\frac{2\pi ik}{r}\cos\theta e^{ikr}\begin{bmatrix} e_0(\bar{k}_s) \\ h_0(\bar{k}_s)\end{bmatrix} \quad (18)$$

with $k_x = k\sin\theta\cos\phi$, $k_y = k\sin\theta\sin\phi$, and $k_{0z} = k\cos\theta$. The field components in the far zone can be approximated as

$$E_\theta \approx -\frac{E_z}{\sin\theta} \quad H_\phi \approx \frac{E_\theta}{\eta} \quad H_\theta \approx -\frac{H_z}{\sin\theta} \quad E_\phi \approx -\eta H_\theta \quad (19)$$

where $\eta$ is the intrinsic impedance of free space.

## 7 Results and discussion

Most of the computer time is spent on calculating the double integral over $k_x$ and $k_y$ in eqns. 12, 16 and 17. The integration path in the $k_x$ ($k_y$) plane is deformed slightly away from the real $k_x$ ($k_y$) axis to avoid possible singularities [4, 6, 19]. At each ($k_x$, $k_y$) pair, a finite difference scheme is performed to calculate the transistion matrix $\bar{P}(\bar{k}_s, z_N, z_0)$, which is time-consuming. The convergence of integration is confirmed by incrementally extending the $k_x$ and $k_y$ integration intervals and observing the evolution of integration results. All computation is done by using a SUN SPARC-10 workstation. Calculating the input impedance at one frequency takes about 15mins.

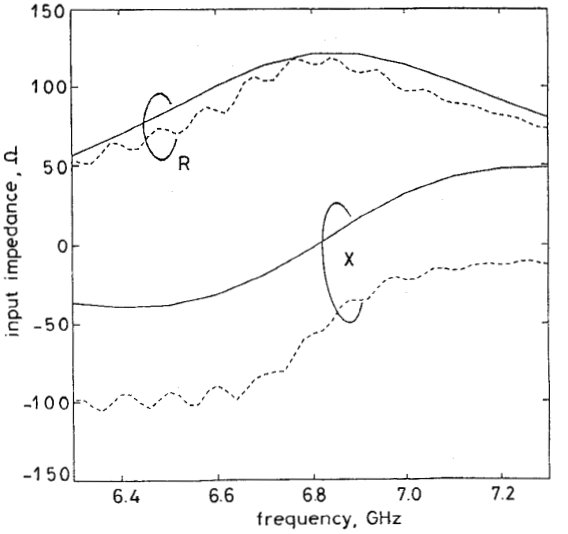


**Fig.2** *Input impedance of a rectangular microstrip antenna*
$a$ = 1.7cm, $b$ = 1.1cm, $d$ = 0.3175cm ($x_s$, $y_s$) = (0.85, 0.15)cm, $\varepsilon_1 = 2.33\,\varepsilon_o$
——— present method
- - - - measurement results from [1]

In Fig. 2, we show the input impedance of a rectangular patch antenna with a thick substrate. Measurements from [1] are also presented for comparison. The real parts match reasonably well, but the imaginary parts have a parallel shift. The authors in [1] pointed out that the imaginary part of their measurement is

shifted due to the inductance in the coaxial feed, which is difficult to remove. Note that the complex conjugate of the input impedance in [1] is shown in Fig. 2 because we use the time convention of $e^{-i\omega t}$.

In Fig. 3, we show the input impedance of a rectangular patch with a thin substrate. The complex conjugate of the input impedance in [2] are used for comparison. The input resistance matches well, but our input reactance has a shift compared to that in [2]. Some error may be incurred when reading the data in [2] because they are presented in a Smith chart with rough scaling. The deviation between our results and those in [2] is comparable to the deviation among the three sets of data presented there.

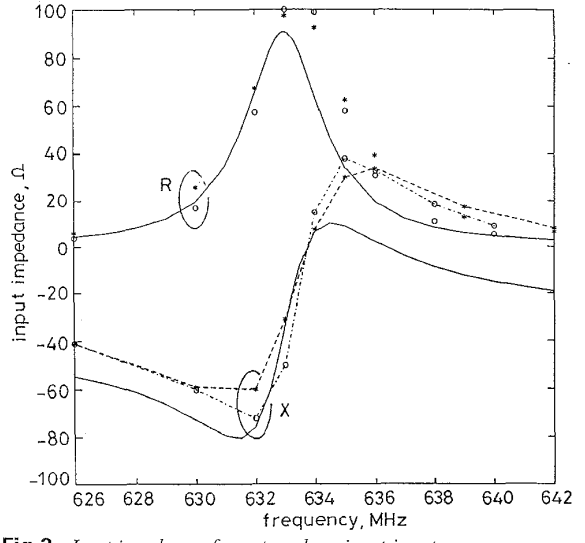


**Fig. 3** *Input impedance of a rectangular microstrip antenna*
$a = 7.5$cm, $b = 15$cm, $d = 0.3175$cm $(x_s, y_s) = (3.75, 6)$cm $\varepsilon_1 = 2.56\ \varepsilon_o$
——— present method
* measurement results from [2]
○ calculated results from [2]
dashed lines connecting * and ○ are for clarity of presentation only

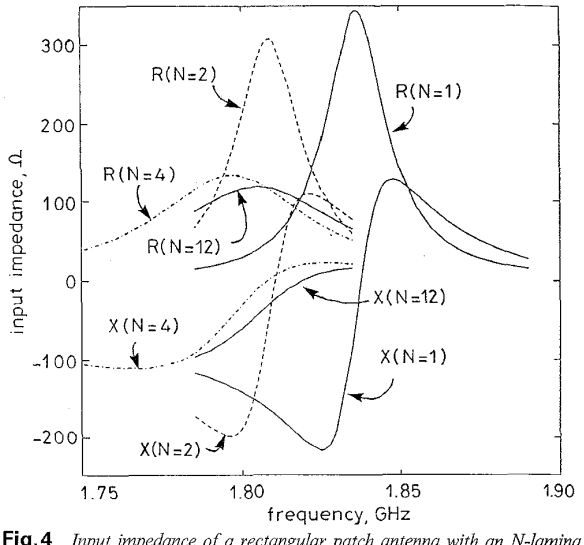


**Fig. 4** *Input impedance of a rectangular patch antenna with an N-lamina composite ground*
$a = 5$cm, $b = 5$cm, $d = 0.15$cm $(x_s, y_s) = (2.5, 0.2)$cm, $R = 1$mm, $\varepsilon_1 = 2.55\ \varepsilon_o$, $\alpha_1 = 0°$, $t_1 = 25\mu$m, $\alpha_2 = 90°$, $t_2 = 25\mu$m, $\sigma'_{xx} = 4 \times 10^4$mho/m, $\sigma'_{yy}$, $= \sigma'_{zz} = 50$mho/m

The self-impedance in eqn. 16 is the input impedance of a dipole in the stratified medium without the presence of the patches. For a short dipole, the input resistance is very small while the input reactance is very large [20], which is why our method predicts a capacitive shift in the thin substrate case. On the other hand, the input reactance obtained by our method approaches zero near resonance in the thick substrate case as in Fig. 2. For the rest of the presentation including Fig. 3, we will include the contribution by the probe feed to the input resistance, but exclude its contribution to the input reactance. For engineering purposes, the input reactance can be compensated by inductive loading. Hence, the reactance shift does not affect the usefulness of our results.

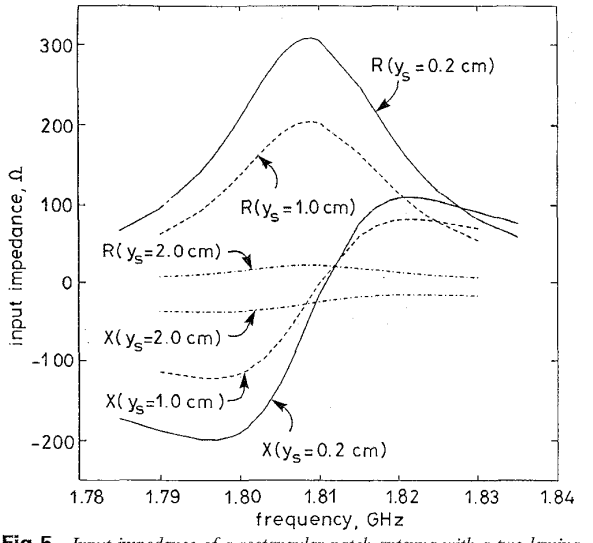


**Fig. 5** *Input impedance of a rectangular patch antenna with a two-lamina composite ground*
$a = 5$cm, $b = 5$cm, $d = 0.15$cm, $x_s = 2.5$cm, $R = 1$mm, $\varepsilon_1 = 2.55\ \varepsilon_o$, $\alpha_1 = 0°$, $t_1 = 25\mu$m, $\alpha_2 = 90°$, $t_2 = 25\mu$m, $\sigma'_{xx} = 4 \times 10^4$mho/m, $\sigma'_{yy}$, $= \sigma'_{zz} = 50$mho/m

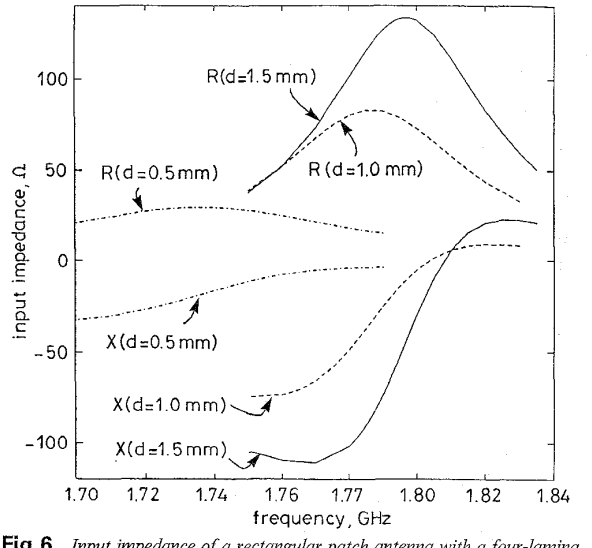


**Fig. 6** *Input impedance of a rectangular patch antenna with a four-lamina composite ground*
$a = 5$cm, $b = 5$cm, $(x_s, y_s) = (2.5, 0.2)$cm, $R = 1$mm, $\varepsilon_1 = 2.55\ \varepsilon_o$, $\alpha_1 = 0°$, $t_1 = 25\mu$m, $\alpha_2 = 90°$, $t_2 = 25\mu$m, $\sigma'_{xx} = 4 \times 10^4$mho/m, $\sigma'_{yy}$, $= \sigma'_{zz} = 50$mho/m

Fig. 4 shows the input impedance of a rectangular patch antenna with a laminated ground plane. The laminated ground consists of $N$ laminae of G/E composite. Each lamina is 25μm thick, the fibre orientation in one lamina is perpendicular to that in the neighbouring one. As the number of laminae increases, both the

input resistance and reactance reduce in magnitude, making it easier to match the input impedance with that of the feeding system. As the number of laminae increases from $N = 2$ to $N = 8$, the resonance frequency shifts and the bandwith increases significantly. However, as the laminae number is further increased from $N = 8$ to $N = 12$, the resonance frequency is only slightly shifted and the bandwidth is almost unchanged. This implies that stacking more composite laminae than $N = 12$ has no further effects. The bandwidth broadening is due to the loss incurred by the conductive composite material. It should also be noted that when $N$ changes from one to two, the resonance frequency shift is close to the magnitude of the bandwidth.

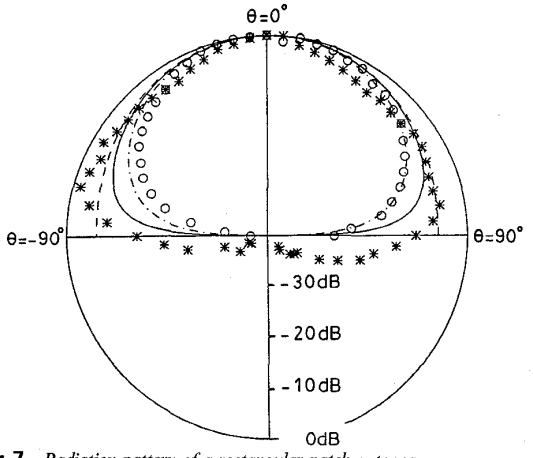


**Fig. 7** *Radiation pattern of a rectangular patch antenna*
——— present approach in *E*-plane (yz-plane)
— - — - present approach in *H*-plane (xz-plane)
- - - - - - *E*-plane [21] * *E*-plane [1] ○ *H*-plane [1]

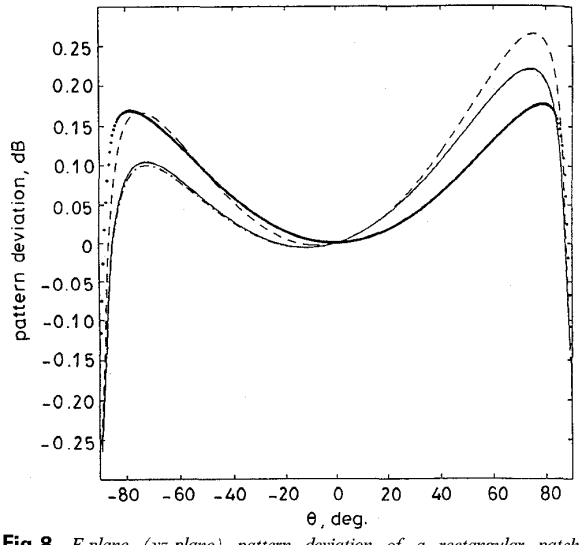


**Fig. 8** *E-plane (yz-plane) pattern deviation of a rectangular patch antenna with an N-lamina composite ground, using pattern with a perfect conductor ground as reference*
All parameters as in Fig. 4
····· $N = 2$ - - - - - $N = 4$ — · — · $N = 8$ ——— $N = 12$

Fig. 5 presents the input impedance with probe location as the parameter. As the probe is moved toward the patch centre, the magnitude of both input resistance and input reactance reduces, and the bandwidth increases. This feature can be used to match the input impedance with that of the feeding system as in conventional microstrip patch antenna design.

Fig. 6 shows the input impedance variation of a rectangular patch antenna as a function of substrate thickness where a four-lamina composite ground is used. When the substrate thickness is reduced, the resonance frequency shifts and the bandwidth is significantly broadened. The broadening is due to the power leakage through the G/E composite. This observation is contrary to the conventional microstrip antennas in which a thicker substrate renders broader bandwidth. The power loss caused by the laminated ground will reduce the radiation efficiency, but is not quantified here.

Fig. 7 shows the field patterns of a rectangular patch antenna. The measurements from [1] and the *E*-plane (*yz* plane) pattern from [21] are also shown for comparison. In the *E*-plane, our result compares favourably with that in [21] around the forward direction ($\hat{z}$ direction). The data of [1] in the backward direction ($-\hat{z}$ direction) is due to the finite ground plane in their experimental setup, and the data of [21] near grazing angles are inaccurate due to the transmission line approximation they used. In the *H*-plane (*xz* plane), our results match reasonably well with those of [1].

Fig. 8 shows the field pattern deviation of a rectangular patch antenna with an *N*-lamina composite ground. The field pattern with a perfect conductor ground is used as the reference. The deviation is asymmetrical and more significant away from the forward direction. The deviations with $N = 8$ and $N = 12$ are almost the same. Note that $\theta = -90°$ indicates the $-\hat{y}$ direction, and $\theta = 90°$ indicates the $\hat{y}$ direction.

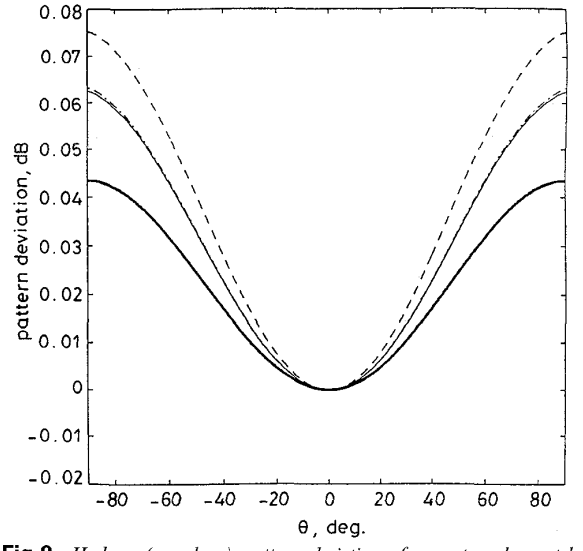


**Fig. 9** *H-plane (xz plane) pattern deviation of a rectangular patch antenna with an N-lamina composite ground using pattern with a perfect conductor ground as reference*
All parameters as in Fig. 4
····· $N = 2$ - - - - - $N = 4$ — · — · $N = 8$ ——— $N = 12$

The field pattern deviations in the *H*-plane are shown in Fig. 9. The deviation is symmetrical and more significant away from the forward direction. The magnitude is less than that in the *E*-plane. The curves with $N = 8$ and $N = 12$ almost overlap. Note that $\theta = -90°$ indicates the $-\hat{x}$ direction, and $\theta = 90°$ indicates the $\hat{x}$ direction.

Fig. 10 shows the pattern deviation in the *E*-plane as a function of the substrate thickness. The substrate thickness of the reference antenna with perfect conductor ground plane is 0.15cm. Around $\theta = \pm 80°$, the pattern deviation with $d = 0.05$cm is about three times

larger than that with $d = 0.15$cm. Around the grazing angle $|\theta| \geq 85°$, the substrate thickness has a much stronger effect on the pattern deviation than the laminated ground. Fig. 11 shows the pattern deviation in the $H$-plane. Near the grazing angle, the pattern deviation with $d = 0.05$cm is about three times larger than that with $d = 0.15$cm, and the deviations are smoother than in the $E$-plane.

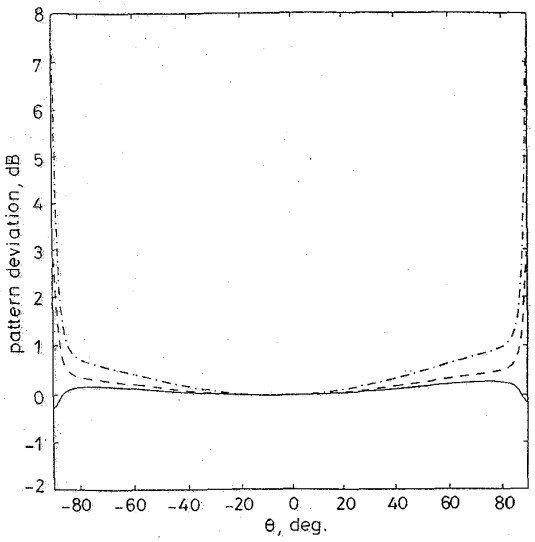


**Fig. 10** *E-plane (yz plane) pattern deviation of a rectangular patch antenna with a four-lamina composite ground, using pattern with a perfect conductor ground as reference*
All parameters as in Fig. 6
——— $d = 0.15$cm - - - - - - $d = 0.1$cm — · — · — $d = 0.05$cm

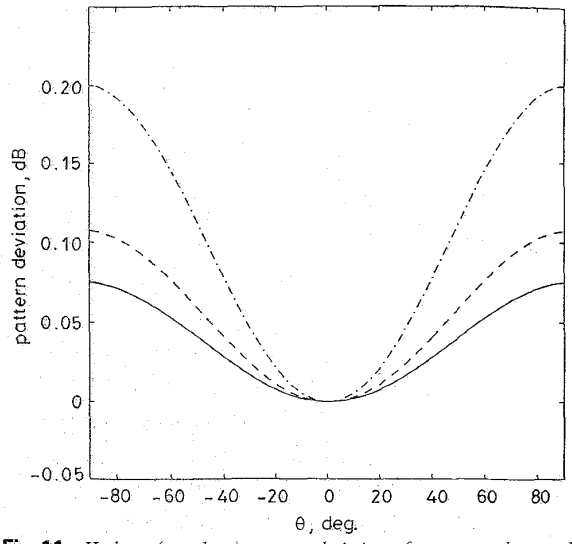


**Fig. 11** *H-plane (xz plane) pattern deviation of a rectangular patch antenna with a four-lamina composite ground, using pattern with a perfect conductor ground as reference*
All parameters as in Fig. 6
——— $d = 0.15$cm - - - - - - $d = 0.1$cm — · — · — $d = 0.05$cm

## 8 Conclusions

We have analysed the radiation characteristics of rectangular patch antennas in the presence of a laminated composite ground plane. Due to the power leakage through the laminated composite, the input impedance decreases and the bandwidth increases when the substrate thickness is reduced. This phenomenon is contrary to the conventional microstrip patch antenna concept, and can be used to design a wideband microstrip patch radiator. The radiation pattern deviation from that with a perfect conductor ground is asymmetrical about the forward direction in the $E$-plane. The deviation is small in the forward direction, and is large near the grazing angles. For the antennas analysed, the pattern deviation caused by laminated ground is of the order of 0.2dB.

## 9 Acknowledgment

The author would like to thank the reviewers for their useful comments.

## 10 References

1 CHANG, E., LONG, S.A., and RICHARDS, W.F.: 'An experimental investigation of electrically thick rectangular microstrip antennas', *IEEE Trans.*, 1986, **AP–34**, (6), pp. 767–772
2 NEWMAN, E.H., and TULYATHAN, P.: 'Analysis of microstrip antennas using moment methods', *IEEE Trans.*, 1981, **AP–29**, (1), pp. 47–53
3 RICHARDS, W.F., LO, Y.T., and HARRISON, D.D.: 'An improved theory for microstrip antennas and applications', *IEEE Trans.*, 1981, **AP–29**, (1), pp. 38–46
4 CHEW, W.C., and LIU, Q.: 'Resonance frequency of a rectangular microstrip patch', *IEEE Trans.*, 1988, **AP–36**, (1), pp. 1045–1056
5 KROWNE, C.M.: 'Relationships for Green's function spectral dyadics involving anisotropic imperfect conductors imbedded in layered anisotropic media', *IEEE Trans.*, 1989, **AP–37**, (9), pp. 1207–1211
6 KIANG, J.-F.: 'Integral equation solution to the skin effect problem in conductor strips of finite thickness', *IEEE Trans.*, 1991, **MTT–39**, (3), pp. 452–460
7 LIN, M.-S., and CHEN, C.H.: 'Plane-wave shielding characteristics of anisotropic laminated composites', *IEEE Trans.*, 1993, **EMC–35**, (1), pp. 21–27
8 MEDGYESI-MITSCHANG, L.N., and PUTNAM, J.M.: 'Scattering from composite laminate strips', *IEEE Trans.*, 1989, **AP–37**, (11), pp. 1427–1436
9 WONG, K.-L., ROW, J.-S., KUO, C.-W., and HUANG, K.-C.: 'Resonance of a rectangular microstrip patch on a uniaxial substrate', *IEEE Trans.*, 1993, **MTT–41**, (4), pp. 698–701
10 HO, T.Q., BEKER, B., SHIH, Y.C., and CHEN, Y.: 'Microstrip resonators on anisotropic substrates', *IEEE Trans.*, 1992, **MTT–40**, (4), pp. 762–765
11 NELSON, R.M., ROGERS, D.A., and D'ASSUNCAO, A.G.: 'Resonant frequency of a rectangular microstrip patch on several uniaxial substrates', *IEEE Trans.*, 1990, **AP–38**, (7), pp. 973–981
12 POZAR, D.M.: 'Radiation and scattering from a microstrip patch on a uniaxial substrate', *IEEE Trans.*, 1987, **AP–35**, (6), pp. 613–621
13 BERREMAN, D.W.: 'Optics in stratified and anisotropic media: 4 × 4-matrix formulation', *J. Opt. Soc. Am.*, 1972, **62**, (4), pp. 502–510
14 SCHWELB, O.: 'Stratified lossy anisotropic media: genearal characteristics', *J. Opt. Soc. Am. A*, 1986, **3**, (2), pp. 188–193
15 MORGAN, M.A., FISHER, D.L., and MILNE, E.A.: 'Electromagnetic scattering by stratified inhomogeneous anisotropic media', *IEEE Trans.*, 1987, **AP–35**, (2), pp. 191–197
16 MESA, F.L., MARQUES, R., and HORNO, M.: 'A general algorithm for computing the bidimensional spectral Green's dyad in multilayered complex bianisotropic media: the equivalent boundary method', *IEEE Trans.*, 1991, **MTT–39**, (9), pp. 1640–1649
17 TSALAMENGAS, J.L., and UZUNOGLU, N.K.: 'Radiation from a dipole in the proximity of a general anisotropic grounded layer', *IEEE Trans.*, 1985, **AP–33**, (2), pp. 165–172
18 KROWNE, C.M.: 'Determination of the Green's function in the spectral domain using a matrix method: application to radiators or resonators immersed in a complex anisotropic layered medium', *IEEE Trans.*, 1986, **AP–34**, (2), pp. 247–253
19 KONG, J.A.: 'Electromagnetic wave theory' (John Wiley, 1990, 2nd edn.)
20 HARRINGTON, R.F.: 'Time-harmonic electromagnetic fields' (McGraw-Hill, New York, 1993) Section 7–9
21 MUNSON, R.E.: 'Microstrip antennas' *in* JOHNSON, R.C. (Ed.) 'Antenna engineering handbook', (McGraw-Hill, New York, 1993, 3rd edn.), Chap. 7